

OpenEM: Large-scale multi-structural 3D datasets for electromagnetic methods

Shuang Wang^{1,2}, Xuben Wang^{1,2}, Fei Deng³, Peifan Jiang^{1,4}, Jian Chen⁵, and Gianluca Fiandaca⁵

¹Key Laboratory of Earth Exploration and Information Techniques of Ministry of Education, Chengdu University of Technology, Chengdu, China.

²College of Geophysics, Chengdu University of Technology, Chengdu, China.

³College of Computer Science and Cyber Security, Chengdu University of Technology, Chengdu, China.

⁴Faculty of Geo-Information Science and Earth Observation, University of Twente, Enschede, Netherlands

⁵The EEM Team for Hydro and eXploration, Department of Earth Sciences “Ardito Desio”, University of Milano, Milano, Italy

Correspondence: Xuben Wang (wxb@cdut.edu.cn)

Abstract. Electromagnetic (EM) methods, owing to their efficiency and non-invasive nature, have become one of the most widely used techniques in geological exploration. Nevertheless, data processing for these methods remains highly time-consuming and labor-intensive. With the remarkable success of deep learning, applying such techniques to EM methods has emerged as a promising research direction to overcome the limitations of conventional approaches. The effectiveness of deep learning methods depends heavily on the quality of datasets, which directly influences model performance and generalization ability. Existing application studies often construct datasets from random one-dimensional or structurally simple three-dimensional models, which fail to represent the complexity of real geological environments. Furthermore, the absence of standardized, publicly available three-dimensional geoelectric datasets continues to hinder progress in deep learning-based EM exploration. To address these limitations, we present OpenEM, a large-scale, multi-structural three-dimensional geoelectric dataset that encompasses a broad range of geologically plausible subsurface structures. OpenEM consists of nine categories of geoelectric models, spanning from simple configurations with anomalous bodies in half-space to more complex structures such as flat layers, folded layers, flat faults, curved faults, and their corresponding variants with anomalous bodies. Since three-dimensional forward modeling in electromagnetics is extremely time-consuming, we further developed a deep learning-based fast forward modeling approach for OpenEM, enabling efficient and reliable forward modeling across the entire dataset. This capability allows OpenEM to be rapidly deployed for a wide range of tasks. OpenEM provides a unified, comprehensive, and large-scale dataset for common EM exploration systems to accelerate the application of deep learning in electromagnetic methods. The complete dataset, along with the forward modeling codes and trained models, is publicly available at <https://doi.org/10.5281/zenodo.17141981> (Wang et al., 2025c).

1 Introduction

Electromagnetic (EM) methods are widely employed in geophysical exploration and remain a central focus of research in the geological exploration industry. A variety of EM systems have been developed, including ground-based, airborne, semi-

airborne, time-domain, and frequency-domain electromagnetic systems. These systems have been extensively applied to geological hazard assessment (Damhuis et al., 2020; Malehmir et al., 2016), groundwater detection (Ball et al., 2020; Minsley et al., 2021), mineral resource exploration (Koné et al., 2021; Okada, 2021), and geological mapping (Dzikunoo et al., 2020; Wong et al., 2020).

The extraction of geoelectric structural information from EM data primarily involves two processes: data processing and inversion (Wu et al., 2022b). Apart from correcting for system response effects, the core task of data processing is denoising. Conventional denoising methods generally depend on empirically chosen parameters, which place heavy demands on the operator's expertise (Wu et al., 2019, 2020). Inversion provides direct insights into the geoelectric structure; however, conventional approaches require iterative corrections through forward modeling, making the process computationally intensive (Siemon et al., 2009; Vallée and Smith, 2009; Vignoli et al., 2015; Christensen et al., 2017). The computational cost increases rapidly with the number of observations, making it unbearable when dealing with large volumes of data (Wu et al., 2023b).

With the rapid development of deep learning, replacing conventional approaches with deep learning techniques to overcome their inherent limitations has gained significant attention and led to numerous practical applications (Huang et al., 2025; Wu et al., 2025a, c). For instance, deep learning has been applied to accelerate forward modeling and mitigate the high computational cost of conventional methods (Bording et al., 2021; Qu et al., 2025; Asif et al., 2021; Wu et al., 2023a), to process acquired data and reduce dependence on empirical expertise (Asif et al., 2025; Wu et al., 2021b; Asif et al., 2022; Li et al., 2024; Wang et al., 2025a), and to perform inversion for efficiently handling large datasets and rapidly obtain subsurface electrical structures (Chen et al., 2022; Wu et al., 2021a; Chen et al., 2025; Wu et al., 2022a, 2024, 2025b). The effectiveness of deep learning methods largely depends on the quality of the dataset, which directly influences both model performance and generalization capability (Wang et al., 2025b). Existing approaches, however, either rely on subsurface resistivity models derived from field data or generate large sets of resistivity models through random or pseudo-random procedures. Training on field-derived resistivity models allows deep learning algorithms to capture geological priors of the target survey area (Bai et al., 2020), but restricts their applicability to that region, limiting generalization to geologically distinct environments. In contrast, randomly generated resistivity models assign resistivity values to each layer based on probability distributions, often resulting in geologically implausible structures (Asif et al., 2023). Consequently, models trained on such dataset struggle to achieve optimal performance.

Therefore, to enhance the performance of deep learning models, improve their ability to process field data, and promote the development of deep learning techniques tailored for electromagnetic methods, a unified, comprehensive, and large-scale resistivity model dataset is urgently required (Bergen et al., 2019; Reichstein et al., 2019). Asif et al. (2023) introduced DL-RMD, a large one-dimensional resistivity dataset that has been widely used in the community for tasks such as denoising (Liu et al., 2024) and inversion (Zhu et al., 2025). However, the real world is inherently three-dimensional, characterized by spatially continuous variations, whereas one-dimensional resistivity models cannot capture complex geological structures such as faults and intrusions (Akingboye, 2025; Teklesenbet, 2012; Melo, 2018). Moreover, due to three-dimensional effects and the interaction between subsurface anomalies and measurement errors, one-dimensional inversion may produce significantly different results at different observation points. Such inconsistencies often lead to poor lateral continuity in inversion profiles

and may even generate spurious anomalies (Yang and Oldenburg, 2012; Oldenburg et al., 2020). To address the limitations of one-dimensional models, researchers have begun exploring three-dimensional inversion with deep learning. Nevertheless, the datasets employed thus far remain relatively simple, typically consisting of half-spaces with anomalies (Tang et al., 2024; Zhang et al., 2025; Zhao et al., 2024). These simplified models fail to adequately represent the wide range of complex geological structures observed in reality, thereby limiting their applicability to field data processing. Furthermore, the lack of a unified and comprehensive three-dimensional resistivity model dataset continues to present a major obstacle to the broader application of deep learning in electromagnetic methods.

To address the limitations and provide a unified, comprehensive, large-scale dataset for advancing the application of deep learning in electromagnetic methods—as well as to supply reliable dataset for field data processing—we present OpenEM, a large-scale, multi-structural, three-dimensional geoelectric model dataset that encompasses a wide range of geologically plausible subsurface structures. OpenEM contains nine categories of geoelectric models with varying levels of complexity, including half-space models with anomalous bodies, flat layers, folded layers, flat faults, curved faults, and their corresponding variants containing anomalous bodies. The resistivity values range from 1 to 2000 $\Omega\cdot\text{m}$, and the models consist of 3 to 7 layers. In models with anomalies, 1 to 5 anomalous bodies of both regular and irregular shapes are incorporated to enhance dataset diversity and realism. In practice, three-dimensional forward modeling is highly time-consuming, which has hindered the broader adoption of deep learning for three-dimensional tasks. To enable efficient use of OpenEM, we further developed a deep learning-based fast forward modeling approach capable of rapidly and reliably generating forward modeling results for the entire dataset. This ensures that OpenEM can be readily applied to a wide range of tasks.

OpenEM is compatible with widely used electromagnetic exploration systems, including ground-based, airborne, semi-airborne, time-domain, and frequency-domain electromagnetic systems. The dataset can be employed to construct surrogate models for well-established processes and supports computationally intensive tasks such as denoising, forward modeling, and inversion. Moreover, OpenEM facilitates research in related areas, including complexity analysis, uncertainty quantification, and generalization studies.

2 Methodology

Geological processes rarely produce random structures, and subsurface resistivity variations are similarly non-random; instead, they typically exhibit spatial correlations, with geological formations largely composed of sedimentary layers. Consequently, randomly generated models are inadequate for realistically representing geological conditions and often fail to satisfy practical requirements. To provide a unified, comprehensive, large-scale dataset that supports the application of deep learning in electromagnetic methods and provides reliable resources for field data processing, we constructed both simple half-space models with anomalies and more complex multi-structural models.

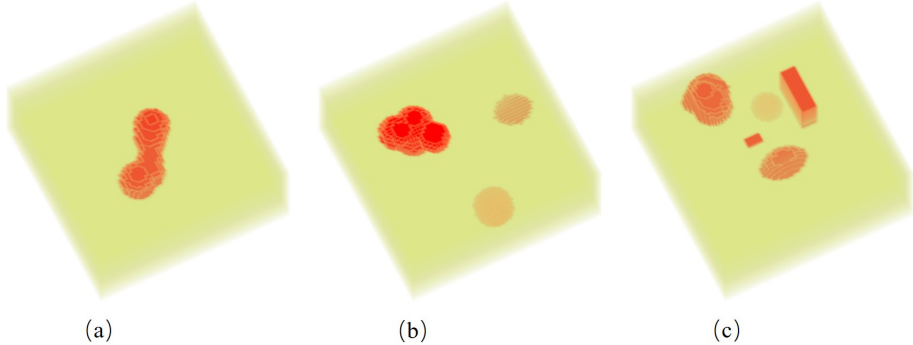


Figure 1. Examples of half-space models: (a) contains one irregular anomaly, (b) contains three anomalies, (c) contains five anomalies.

2.1 Half-space models with anomalies

For the half-space models, background resistivity is set between 100 and 1000 $\Omega\cdot\text{m}$ in increments of 100 $\Omega\cdot\text{m}$, while anomaly resistivity ranges from 1 to 2000 $\Omega\cdot\text{m}$. Anomalies are categorized into regular anomalies and irregular anomalies. Regular anomalies include quadrangular prisms, triangular prisms, spheres, and ellipsoids. The number of anomalies is randomly assigned between 1 and 5. Fig. 1 shows three examples of half-space models containing 1, 3, and 5 anomalies, illustrating both regular and irregular types.

2.2 Multi-structure models

To generate geologically plausible models, we employed von Kármán covariance functions (Møller et al., 2001) to create the initial layered geological structures.

$$r = A^2 C \left(\frac{z}{L} \right)^\nu K_\nu \left(\frac{z}{L} \right) \quad (1)$$

Where, A represents the amplitude of the logarithmic resistivity, C is the scale factor, z denotes the spatial (vertical) distance, L is the maximum correlation length considered, and K is the modified Bessel function of the second kind with order ν .

The generated initial layered model is presented in Fig. 2a. Building on this model, geological structures such as faults and folds are iteratively incorporated. Letting the initial layered model be denoted as r_0 , faults are introduced through iterative updates according to the following mathematical formulation:

$$r_i(x, y, z) = \begin{cases} r_0(a_i \sin(2\pi k_i x) + s_i, a_i \sin(2\pi k_i y) + s_i, z + s'_i), & z \geq f_i(x, y) \\ r_{i-1}(x, y, z), & z < f_i(x, y) \end{cases}; \quad i > 0 \quad (2)$$

Where, s_i , s'_i , k_i , and a_i are the random variables at the i -th iteration. $f_i(x, y)$ denotes a random curve used for fault simulation.

$$f_i(x, y) = c_i x + d_i y + A_1 \sin(\omega_1 x + \phi_1) + A_2 \cos(\omega_2 y + \phi_2) + e_i \quad (3)$$

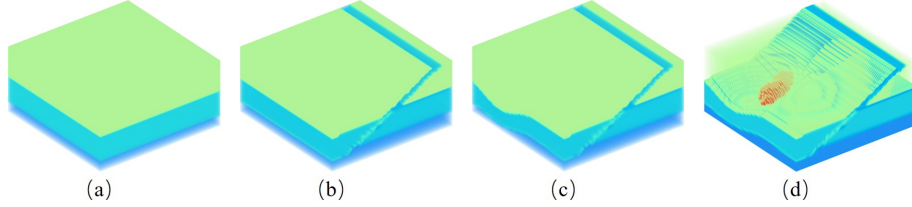


Figure 2. Model construction process: (a) initial layered model, (b) model with added faults, (c) model with added folded strata, and (d) model with embedded anomalies.

Where c_i , d_i , A_1 , A_2 , ω_1 , ω_2 , ϕ_1 , ϕ_2 , and e_i denote the random variables at the i -th iteration, and the model after incorporating faults is illustrated in Fig. 2b. Once the fault structures are established, folds are subsequently introduced into the model, which are simulated using the following mathematical formulation:

$$r_i(x, y, z) = r_{i-1}(x, a_i \sin(2\pi k_i x), a_i \sin(2\pi k_i x)); \quad i > 0 \quad (4)$$

The model after incorporating folds is illustrated in Fig. 2c.

Through the construction process described above, layered geological models containing faults and folds are generated. Alternatively, one or two of these steps can be applied independently to create different types of geological models. To simulate resistivity variations induced by local anomalies, 1 to 5 anomalies are subsequently introduced into the model. Their scales are consistent with those used in the half-space models and are classified as either irregular or regular. Regular anomalies primarily include quadrangular prisms, triangular prisms, spheres, and ellipsoids. The number of anomalies is randomly assigned between 1 and 5. The model with anomalies added is illustrated in Fig. 2d.

3 OpenEM

OpenEM consists of nine types of geological models, as illustrated in Fig. 3. These models range from simple to complex and include half-space models with anomalies, layered models, layered models with faults, folded models, folded models with faults, and their respective variants containing anomalies. Each type comprises approximately 120,000 models, yielding a total of about 1.08 million models in OpenEM. Collectively, these models capture the majority of geological scenarios encountered in practice. The key features of OpenEM are summarized in Table 1.

Table 1. OpenEM model information

	Number	Resistivity	Number of layer	Number of anomaly
OpenEM	1,080,000	1-2000	3-7	1-5

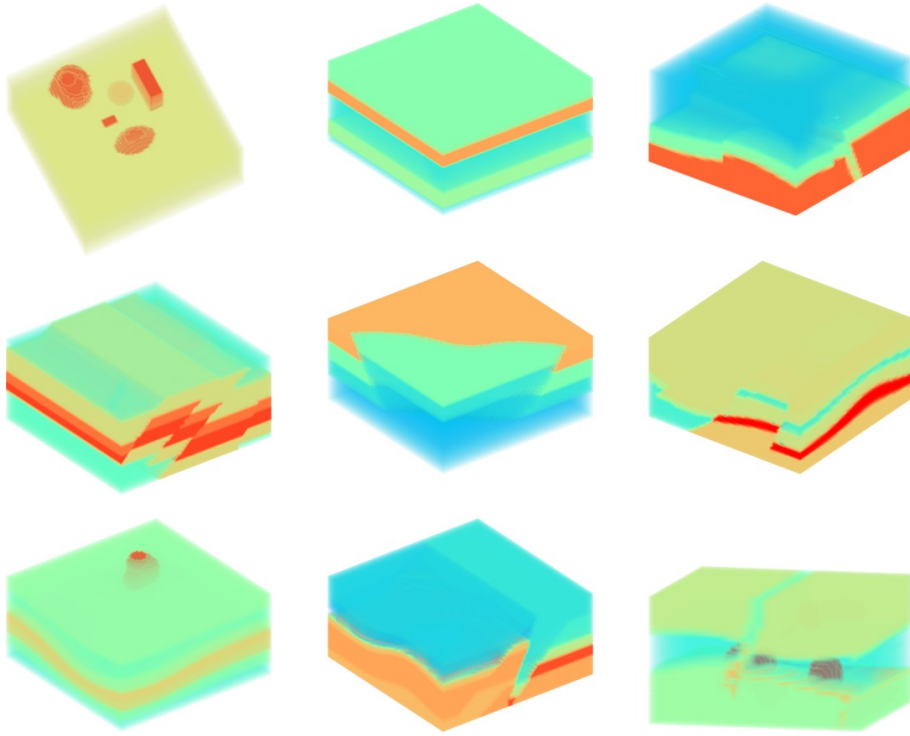


Figure 3. Examples of OpenEM models, illustrating the nine types included in OpenEM.

The statistical characteristics of OpenEM are presented in Fig. 4. Fig. 4a depicts the overall resistivity distribution, which is approximately uniform but slightly skewed toward lower resistivity values. This distribution is favorable for electromagnetic methods, as their resolution is generally higher in low-resistivity regions (Jørgensen et al., 2005). Fig. 4b shows the statistics of the number of layers in layered models, where the layer count is uniformly distributed between 3 and 7. Fig. 4c illustrates the statistics of anomaly counts, indicating that the number of anomalies ranges from 1 to 5 and follows a uniform distribution.

4 Forward

When applying OpenEM in practical applications, it is necessary to perform forward modeling on the models to generate usable labels. However, forward modeling of three-dimensional models is computationally expensive, which presents challenges for practical applications. To overcome this limitation, we developed a deep learning–based fast forward modeling method tailored to the widely used AeroTEM IV system (Bedrosian et al., 2014), enabling efficient forward modeling of OpenEM.

4.1 Network architecture

The objective is to provide a fast forward modeling tool capable of efficiently handling three-dimensional models. The overall framework of the method is illustrated in Fig. 5.

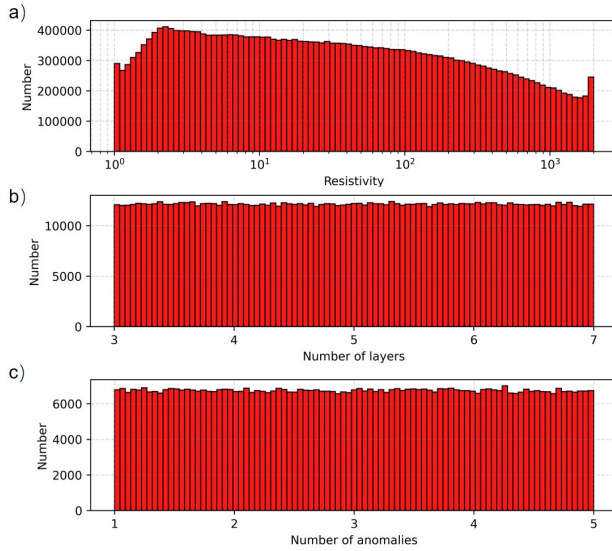


Figure 4. Statistical information of OpenEM. (a) Resistivity distribution, (b) Number of layer distribution, (c) number of anomaly distribution.

The network takes three-dimensional geoelectrical models as input and produces the corresponding forward modeling data as output. To account for altitude-related variations, a dedicated embedding is introduced for the transmitter–receiver altitude. The overall architecture follows a 3D U-Net framework that integrates attention mechanisms with altitude embedding. The encoder consists of a series of DownBlock and DownSample modules, where the DownBlocks progressively increase the number of channels while preserving spatial resolution. The decoder is composed of UpBlock and UpSample modules. A key feature of the design is that each DownBlock and UpBlock incorporates the altitude embedding, embedding transmitter–receiver height information as prior knowledge into multiple layers of the network. This design significantly enhances the model’s ability to capture altitude-dependent features and improves the accuracy of forward predictions.

The DownBlock and UpBlock share the same structure, each comprising a ResBlock, an altitude embedding, and an AttentionBlock. The ResBlock contains two three-dimensional convolutional layers with residual connections. The altitude embedding incorporates the transmitter–receiver height into the network, while the AttentionBlock applies the attention mechanism.

4.2 Train

A total of 10,000 models were randomly selected from OpenEM for forward modeling, uniformly sampled across nine types of geological models. The dataset was then divided into training, validation, and test subsets in an 8:1:1 ratio.

For forward modeling, the models were discretized on a uniform grid with a spacing of 10 m, yielding network inputs of size $64 \times 64 \times 32$. Transmitter heights ranged from 25 to 100 m, representing typical flight conditions. The forward modeling

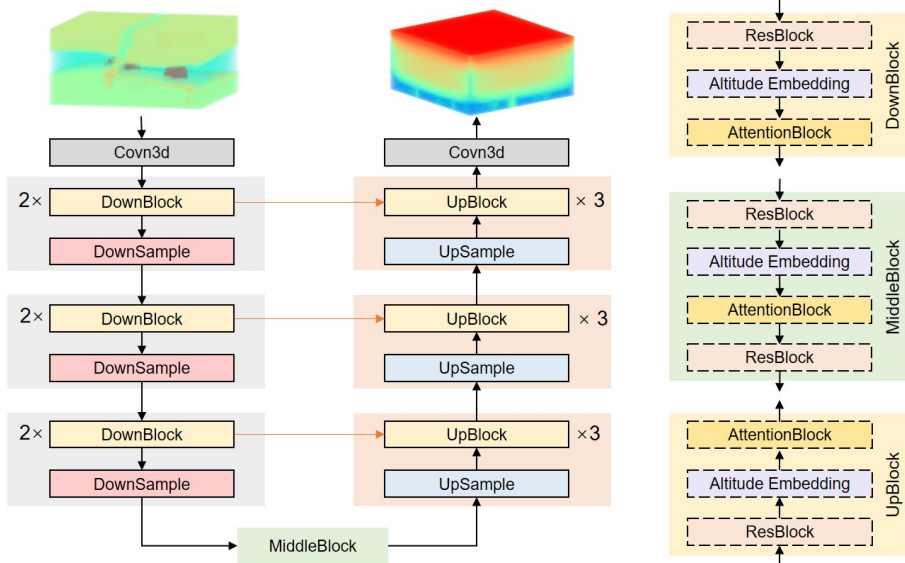


Figure 5. Forward modeling network architecture, with the overall structure shown on the left and detailed module information on the right.

was conducted according to the specifications of the AeroTEM IV system, including the transmitter current and receiver configuration. The corresponding responses were computed using the SimPEG forward modeling framework (Cockett et al., 2015). The observation system was uniformly distributed, consisting of 32 survey lines, each with 32 measurement points, and 32 selected time samples, resulting in output responses of size $32 \times 32 \times 32$.

The network was trained for 200 epochs on a single NVIDIA A6000 GPU using the AdamW optimizer with a learning rate of 0.0001.

4.3 Test

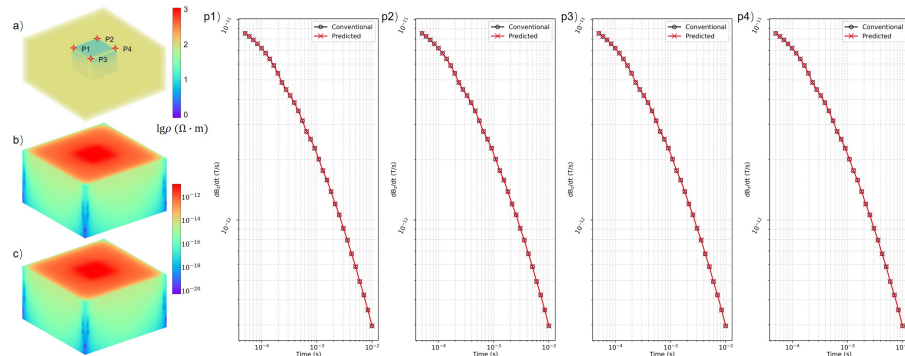


Figure 6. Simple model test: (a) geoelectric model, (b) network-predicted results, (c) forward modeling results using the conventional method, and (P1)–(P4) correspond to the 1D responses at the four points indicated in (a).

We first evaluated the method on a simple half-space model containing a low-resistivity anomaly, as shown in Fig. 6. The forward modeling results obtained with the conventional approach and the proposed method are presented in Fig. 6. The results show that the proposed method accurately predicts the overall forward response, demonstrating strong consistency and effectively capturing the characteristics of the low-resistivity anomaly. To enable a more detailed comparison, four points above the anomaly body were selected, as shown in Fig. 6p1-p4. The network-predicted responses closely match those computed with the conventional method.

To quantitatively assess the network's predictions, we computed the relative errors between the network-predicted results and those obtained from conventional forward modeling, as shown in Table 2. The results show that the overall relative error is less than 1%, indicating that the network can accurately reproduce the forward responses of the models.

Table 2. Relative error between network-predicted forward responses and conventional forward modeling results for the simple model.

	All	P1	P2	P3	P4
Relative error (%)	0.81	0.68	0.45	0.52	0.86

To assess the network's ability to handle complex models, we evaluated it on the most challenging model type. A randomly selected example is shown in Fig. 7a, which features faults, folds, and high-resistivity anomalies. The corresponding network-predicted results are presented in Fig. 7b. Even for such complex geological structures, the network accurately predicts the forward responses, demonstrating high reliability. For detailed comparison, four points were selected, as shown in Fig. 7p1-p4. The network-predicted responses closely match the numerical results from the conventional method, confirming the robustness of the network.

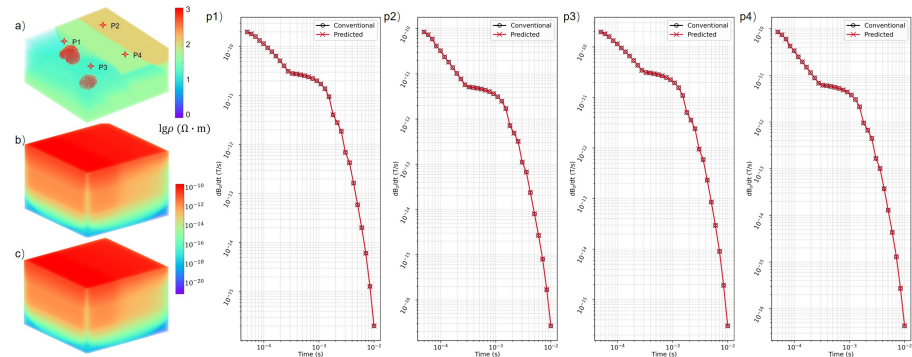


Figure 7. Simple model test: (a) geoelectric model, (b) network-predicted results, (c) forward modeling results using the conventional method, and (P1)–(P4) correspond to the 1D responses at the four points indicated in (a).

Table 3 summarizes the overall relative error for the complex models as well as the errors at the four specific comparison points. For complex models, the relative error increases slightly, with the maximum value of 1.43% at point P1 and an overall

error of 1.24%, both remaining below 2%. These results indicate that the network can still accurately predict the forward responses of complex geological models.

Table 3. Relative error between network-predicted forward responses and conventional forward modeling results for the complex model.

	All	P1	P2	P3	P4
Relative error (%)	1.24	1.43	0.77	0.90	0.83

To further assess the reliability of the network, we calculated the relative errors between the network-predicted results and those obtained from conventional forward modeling across the entire test set, as shown in Fig. 8. The maximum relative error is 6.3%, while 99% of the models have relative errors below 5%, with a mean of 0.92%. These results demonstrate that the network effectively captures the mapping between geological models and their forward responses, making it suited for rapid forward modeling.

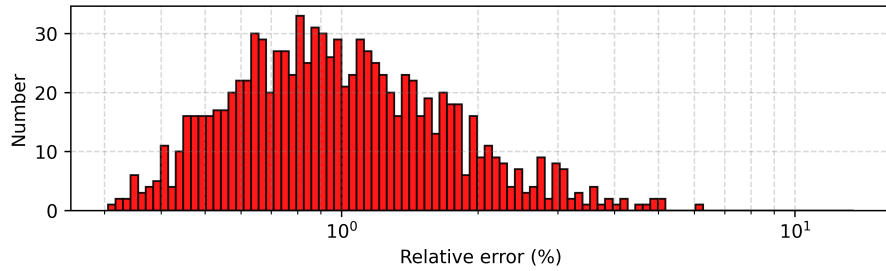


Figure 8. Relative error between network-predicted forward responses and conventional forward modeling results on the test set.

5 Discussion

As a large-scale, multi-structural dataset, OpenEM can substantially advance the application of deep learning in electromagnetic studies. Networks trained on OpenEM outperform those trained on random resistivity models or simple half-space models, as geological structures are inherently diverse and variable. OpenEM's nine major structural model types cover the majority of geological scenarios from simple to complex, allowing networks trained on OpenEM to achieve more accurate and satisfactory results.

The resistivity range of OpenEM spans from 1 to 2000 $\Omega\cdot\text{m}$, encompassing most geological scenarios. In some formations, however, resistivity can exceed 2000 $\Omega\cdot\text{m}$, as observed in certain granites and basalts. Nevertheless, electromagnetic methods exhibit limited sensitivity and low resolution in such high-resistivity environments. Therefore, we set 2000 $\Omega\cdot\text{m}$ as the upper resistivity limit.

Three-dimensional forward modeling in electromagnetic methods is computationally intensive, which constrains the development of deep learning approaches for 3D applications. So, we developed a deep learning model for OpenEM that enables fast forward modeling and achieves reliable results with a relative error of less than 5%. This margin of error is acceptable, as the uncertainty in measured field data is generally much higher than that introduced by forward modeling.

The current forward modeling simulator was specifically developed for the widely used AeroTEM IV system. Consequently, when applied to other systems, such as VTEM, the network may show a certain degree of incompatibility. This issue can be mitigated through small-scale transfer learning, as the network has already captured the fundamental patterns of forward responses. Compared with large-scale training, such transfer learning demands substantially fewer computational resources.

6 Code and data availability

The complete dataset, along with the forward modeling codes and trained models, is publicly available at <https://doi.org/10.5281/zenodo.17141981> (Wang et al., 2025c). The forward modeling code is also openly available at <https://github.com/WAL-l/OpenEM>.

7 Conclusions

This paper introduces OpenEM, a large-scale, multi-structural three-dimensional geoelectrical model dataset. The resistivity values range from 1 to 2000 $\Omega\cdot\text{m}$, and the structures include common geological features such as faults, folds, and various anomalies. Each model contains 3 to 7 layers, and in models with anomalies, 1 to 5 anomalies of both regular and irregular shapes are randomly distributed, thereby enhancing the dataset's diversity and geological representativeness. To overcome the computational expense of three-dimensional forward modeling in electromagnetic methods, we developed a fast forward modeling approach for OpenEM, tailored to the widely used AeroTEM IV system. The proposed network enables rapid and reliable forward modeling of three-dimensional models, facilitating the efficient application of OpenEM to diverse tasks. Furthermore, OpenEM is compatible with widely used ground-based, airborne, semi-airborne, time-domain, and frequency-domain electromagnetic systems, and is intended to provide a unified, comprehensive, large-scale dataset to promote the advancement of deep learning applications in electromagnetic research.

Author contributions. TEXT

Competing interests. The authors declare that they have no conflict of interest.

Acknowledgements. TEXT

References

Akingboye, A. S.: Electrical and seismic refraction methods: Fundamental concepts, current trends, and emerging machine learning prospects, *Discover Geoscience*, 3, 87, 2025.

Asif, M. R., Bording, T. S., Barfod, A. S., Grömbacher, D. J., Maurya, P. K., Christiansen, A. V., Auken, E., and Larsen, J. J.: Effect of data pre-processing on the performance of neural networks for 1-D transient electromagnetic forward modeling, *IEEE Access*, 9, 34 635–34 646, 2021.

Asif, M. R., Maurya, P. K., Foged, N., Larsen, J. J., Auken, E., and Christiansen, A. V.: Automated transient electromagnetic data processing for ground-based and airborne systems by a deep learning expert system, *IEEE Transactions on Geoscience and Remote Sensing*, 60, 1–14, 2022.

Asif, M. R., Foged, N., Bording, T., Larsen, J. J., and Christiansen, A. V.: DL-RMD: a geophysically constrained electromagnetic resistivity model database (RMD) for deep learning (DL) applications, *Earth System Science Data*, 15, 1389–1401, 2023.

Asif, M. R., Kass, M. A., Herpe, M., Rawlinson, Z., Westerhoff, R., Larsen, J. J., and Christiansen, A. V.: Comparative analysis of deep learning and traditional airborne electromagnetic data processing: A case study, *Geophysics*, 90, WA103–WA112, 2025.

Bai, P., Vignoli, G., Viezzoli, A., Nevalainen, J., and Vacca, G.: (Quasi-) real-time inversion of airborne time-domain electromagnetic data via artificial neural network, *Remote Sensing*, 12, 3440, 2020.

Ball, L. B., Bedrosian, P. A., and Minsley, B. J.: High-resolution mapping of the freshwater–brine interface using deterministic and Bayesian inversion of airborne electromagnetic data at Paradox Valley, USA, *Hydrogeology Journal*, 28, 941–954, 2020.

Bedrosian, P. A., Ball, L. B., and Bloss, B. R.: Airborne Electromagnetic Data and Processing Within Leech Lake Basin, Fort Irwin, California, US Department of the Interior, US Geological Survey, 2014.

Bergen, K. J., Johnson, P. A., de Hoop, M. V., and Beroza, G. C.: Machine learning for data-driven discovery in solid Earth geoscience, *Science*, 363, eaau0323, 2019.

Bording, T. S., Asif, M. R., Barfod, A. S., Larsen, J. J., Zhang, B., Grömbacher, D. J., Christiansen, A. V., Engebretsen, K. W., Pedersen, J. B., Maurya, P. K., et al.: Machine learning based fast forward modelling of ground-based time-domain electromagnetic data, *Journal of Applied Geophysics*, 187, 104 290, 2021.

Chen, J., Zhang, Y., and Lin, T.: Transient electromagnetic machine learning inversion based on pseudo wave field data, *IEEE Transactions on Geoscience and Remote Sensing*, 60, 1–10, 2022.

Chen, J., Galli, S., Signora, A., Sullivan, N. A. L., Zhang, B., and Fiandaca, G.: Rapid Bayesian Imaging of Large-Scale Transient Electromagnetic Data Using Probabilistic Neural Networks, *Journal of Geophysical Research: Machine Learning and Computation*, 2, e2024JH000 536, 2025.

Christensen, N. K., Ferre, T. P. A., Fiandaca, G., and Christensen, S.: Voxel inversion of airborne electromagnetic data for improved ground-water model construction and prediction accuracy, *Hydrology and Earth System Sciences*, 21, 1321–1337, 2017.

Cockett, R., Kang, S., Heagy, L. J., Pidlisecky, A., and Oldenburg, D. W.: SimPEG: An open source framework for simulation and gradient based parameter estimation in geophysical applications, *Computers & Geosciences*, 85, 142–154, 2015.

Damhuis, R. M., Roux, P. L., and Fourie, C. J.: The identification and mitigation of geohazards using shallow airborne engineering geophysics and land-based geophysics for brown-and greenfield road investigations, *Quarterly Journal of Engineering Geology and Hydrogeology*, 53, 321–332, 2020.

Dzikunoo, E. A., Vignoli, G., Jørgensen, F., Yidana, S. M., and Banoeng-Yakubo, B.: New regional stratigraphic insights from a 3D geological model of the Nasia sub-basin, Ghana, developed for hydrogeological purposes and based on reprocessed B-field data originally collected for mineral exploration, *Solid Earth*, 11, 349–361, 2020.

Huang, Q., Wu, S., and Xue, J.: Data Science and Machine Learning in Geo-Electromagnetics: A Review, *Surveys in Geophysics*, pp. 1–56, 2025.

Jørgensen, F., Sandersen, P. B., Auken, E., Lykke-Andersen, H., and Sørensen, K.: Contributions to the geological mapping of Mors, Denmark—a study based on a large-scale TEM survey, *Bulletin of the Geological Society of Denmark*, 52, 53–75, 2005.

Koné, A. Y., Nasr, I. H., Traoré, B., Amiri, A., Inoubli, M. H., Sangaré, S., and Qaysi, S.: Geophysical contributions to gold exploration in western Mali according to airborne electromagnetic data interpretations, *Minerals*, 11, 126, 2021.

Li, G., Wu, S., Cai, H., Chen, C., Chen, H., Xiao, D., and Yan, J.: GTCN: Gated Temporal Convolutional Networks for Controlled-Source Electromagnetic Data Denoising, *IEEE Transactions on Geoscience and Remote Sensing*, 2024.

Liu, Y., Zhang, Y., Guo, C., Zhang, S., Kang, H., and Zhao, Q.: A multi-task learning network based on the Transformer network for airborne electromagnetic detection imaging and denoising, *Journal of Geophysics and Engineering*, 21, 1056–1070, 2024.

Malehmir, A., Socco, L. V., Bastani, M., Krawczyk, C. M., Pfaffhuber, A. A., Miller, R. D., Maurer, H., Frauenfelder, R., Suto, K., Bazin, S., et al.: Near-surface geophysical characterization of areas prone to natural hazards: a review of the current and perspective on the future, *Advances in Geophysics*, 57, 51–146, 2016.

Melo, A. T.: Integrated quantitative interpretation of multiple geophysical data for geology differentiation, *Colorado School of Mines*, 2018.

Minsley, B. J., Rigby, J. R., James, S. R., Burton, B. L., Knierim, K. J., Pace, M. D., Bedrosian, P. A., and Kress, W. H.: Airborne geophysical surveys of the lower Mississippi Valley demonstrate system-scale mapping of subsurface architecture, *Communications Earth & Environment*, 2, 131, 2021.

Møller, I., Jacobsen, B. H., and Christensen, N. B.: Rapid inversion of 2-D geoelectrical data by multichannel deconvolution, *Geophysics*, 66, 800–808, 2001.

Okada, K.: A historical overview of the past three decades of mineral exploration technology, *Natural Resources Research*, 30, 2839–2860, 2021.

Oldenburg, D. W., Heagy, L. J., Kang, S., and Cockett, R.: 3D electromagnetic modelling and inversion: a case for open source, *Exploration Geophysics*, 51, 25–37, 2020.

Qu, Z., Gao, Y., Xing, K., and Zhang, X.: Deep-TEMNet: A Hybrid U-Net–2D LSTM Network for Efficient and Accurate 2.5 D Transient Electromagnetic Forward Modeling, *Remote Sensing*, 17, 264, 2025.

Reichstein, M., Camps-Valls, G., Stevens, B., Jung, M., Denzler, J., Carvalhais, N., and Prabhat, F.: Deep learning and process understanding for data-driven Earth system science, *Nature*, 566, 195–204, 2019.

Siemon, B., Auken, E., and Christiansen, A. V.: Laterally constrained inversion of helicopter-borne frequency-domain electromagnetic data, *Journal of Applied Geophysics*, 67, 259–268, 2009.

Tang, R., Gan, L., Li, F., and Shen, F.: A Fast Three-dimensional Imaging Scheme of Airborne Time Domain Electromagnetic Data using Deep Learning, *Authorea Preprints*, 2024.

Teklesenbet, A.: Multidimensional inversion of MT data from Alid Geothermal area, Eritrea. Comparison with geological structures and identification of a geothermal reservoir, Ph.D. thesis, 2012.

Vallée, M. A. and Smith, R. S.: Inversion of airborne time-domain electromagnetic data to a 1D structure using lateral constraints, *Near Surface Geophysics*, 7, 63–71, 2009.

Vignoli, G., Fiandaca, G., Christiansen, A. V., Kirkegaard, C., and Auken, E.: Sharp spatially constrained inversion with applications to transient electromagnetic data, *Geophysical Prospecting*, 63, 243–255, 2015.

Wang, S., Guo, M., Wang, X., Deng, F., Mao, L., Wang, B., and Gao, W.: DREMnet: An Interpretable Denoising Framework for Semi-Airborne Transient Electromagnetic Signal, *arXiv preprint arXiv:2503.22223*, 2025a.

Wang, S., Wang, X., and Deng, F.: Interpretable deep learning paradigm for airborne transient electromagnetic inversion, in: SEG Near-Surface Geophysical Exploration and Geo-Disaster Prevention Technology Workshop, Chengdu, China, July 4–6, 2025, pp. 51–52, Society of Exploration Geophysicists, 2025b.

Wang, S., Wang, X., Deng, F., Jiang, P., Chen, J., and Gianluca, F.: OpenEM: Large-scale multi-structural 3D datasets for electromagnetic methods, *Zenodo*, <https://doi.org/10.5281/zenodo.17141981>, 2025c.

Wong, S. C., Ley-Cooper, Y., Rollet, N., Brodie, R. C., Bonnardot, M.-A., English, P., Nicoll, M., and Roach, I.: Interpretation of the AusAEM1: Insights from the world's largest airborne electromagnetic survey, *Geoscience Australia*, 2020.

Wu, S., Huang, Q., and Zhao, L.: Convolutional neural network inversion of airborne transient electromagnetic data, *Geophysical Prospecting*, 69, 1761–1772, 2021a.

Wu, S., Huang, Q., and Zhao, L.: De-noising of transient electromagnetic data based on the long short-term memory-autoencoder, *Geophysical Journal International*, 224, 669–681, 2021b.

Wu, S., Huang, Q., and Zhao, L.: Instantaneous inversion of airborne electromagnetic data based on deep learning, *Geophysical Research Letters*, 49, e2021GL097165, 2022a.

Wu, S., Huang, Q., and Zhao, L.: A deep learning-based network for the simulation of airborne electromagnetic responses, *Geophysical Journal International*, 233, 253–263, 2023a.

Wu, S., Huang, Q., and Zhao, L.: Fast Bayesian inversion of airborne electromagnetic data based on the invertible neural network, *IEEE Transactions on Geoscience and Remote Sensing*, 61, 1–11, 2023b.

Wu, S., Huang, Q., and Zhao, L.: Physics-guided deep learning-based inversion for airborne electromagnetic data, *Geophysical Journal International*, 238, 1774–1789, 2024.

Wu, S., Deng, S., Wei, X., Rizwan Asif, M., Vignoli, G., and Farquharson, C. G.: Frontiers in electromagnetic geophysics—Introduction, 2025a.

Wu, S., Sun, J., and Chen, J.: Variational inference for geophysical Bayesian inverse problems using normalizing flows: An unsupervised approach to electromagnetic data inversion, *Geophysical Journal International*, p. ggaf239, 2025b.

Wu, S., Thoram, S., Sun, J., Sager, W., and Chen, J.: Characterizing marine magnetic anomalies: A machine learning approach to advancing the understanding of oceanic crust formation, *Journal of Geophysical Research: Solid Earth*, 130, e2024JB030682, 2025c.

Wu, X., Xue, G., Xiao, P., Li, J., Liu, L., and Fang, G.: The removal of the high-frequency motion-induced noise in helicopter-borne transient electromagnetic data based on wavelet neural network, *Geophysics*, 84, K1–K9, 2019.

Wu, X., Xue, G., He, Y., and Xue, J.: Removal of multisource noise in airborne electromagnetic data based on deep learning, *Geophysics*, 85, B207–B222, 2020.

Wu, X., Xue, G., Zhao, Y., Lv, P., Zhou, Z., and Shi, J.: A deep learning estimation of the earth resistivity model for the airborne transient electromagnetic observation, *Journal of Geophysical Research: Solid Earth*, 127, e2021JB023185, 2022b.

Yang, D. and Oldenburg, D. W.: Three-dimensional inversion of airborne time-domain electromagnetic data with applications to a porphyry deposit, *Geophysics*, 77, B23–B34, 2012.

Zhang, S., Liu, R., Feng, H., Wang, Z., Liu, S., Luo, Y., Zheng, Z., and Sun, H.: 3D inversion of airborne transient electromagnetic data using deep learning, *Journal of Applied Geophysics*, 239, 105 737, 2025.

Zhao, Y., Wu, X., Chen, W., Xue, J., and Shi, J.: Three-dimensional inversion for short-offset transient electromagnetic data based on 3D U-Net, *Journal of Geophysics and Engineering*, 21, 922–937, 2024.

Zhu, Y., Tang, Y., Li, J., Hu, X., and Peng, R.: A Deep Learning Approach for Transient Electromagnetic Data Denoising, Inversion and Uncertainty Analysis With Monte Carlo Dropout Technique, *Geophysical Prospecting*, 73, e70 069, 2025.